Structure Functions and Structure Parameters of Velocity Fluctuations in Numerically Simulated Atmospheric Convective Boundary Layer Flows

JEREMY A. GIBBS[a,b] AND EVGENI FEDOROVICH[c]

[a] *Cooperative Institute for Mesoscale Meteorological Studies, University of Oklahoma, Norman, Oklahoma;* [b] *NOAA/OAR/National Severe Storms Laboratory, Norman, Oklahoma;* [c] *School of Meteorology, University of Oklahoma, Norman, Oklahoma*

ABSTRACT: We extend our previous study, which dealt with structure functions of potential temperature fluctuations, and focus on the characteristics of second-order velocity structure functions and corresponding structure parameters in the atmospheric convective boundary layer. We consider the three previously reported methods to compute the structure parameters of turbulent velocity fields: the direct method, the true spectral method, and the approximate spectral method. The methods are evaluated using high-resolution gridded numerical data from large-eddy simulations of shear-free and shear-driven convective boundary layers. Results indicate that the direct and true spectral methods are more suitable than the approximate spectral method, which overestimates the structure parameters of velocity as a result of assuming the inertial-subrange shape of the velocity spectrum for all turbulence scales. Results also suggest that structure parameters of vertical velocity fluctuations are of limited utility because of violations of local isotropy, especially in shear-free convective boundary layers.

KEYWORDS: Turbulence; Boundary layer

1. Introduction

The structure function of a random turbulent field represents the intensity of fluctuations with spatial length scales that are smaller than, or on the order of, a prescribed separation distance (Kolmogorov 1941a,b; Tatarskii 1961). Examples of random fields in the atmosphere include spatial distributions of meteorological variables such as temperature, humidity, velocity, and refractive index of the air. For many applications associated with atmospheric boundary layer processes, it is customary to characterize turbulent fluctuations within the inertial subrange of turbulence scales through a single representative parameter called the structure-function (or structure) parameter. It enables the description of the turbulence fluctuations in terms of a single quantity by removing the explicit dependence on a separation distance.

Properties of structure parameters for scalars have been historically discussed in the literature more than those for velocity (e.g., Wyngaard et al. 1971; Burk 1980; Andreas 1988; Peltier and Wyngaard 1995; Frederickson et al. 2000; Wilson and Fedorovich 2012; Wainwright et al. 2015), although the topic has been addressed (e.g., Lesieur and Metais 1996; Rizza et al. 2006, 2010). This is apparently because the parameters of scalar fluctuations (particularly, fluctuations of temperature and humidity) are essential for designing atmospheric measurement techniques, such as scintillometry, and for understanding the physics of atmospheric acoustic and electromagnetic wave propagation, which is fundamental for remote sensing applications. The idea of using structure functions to describe atmospheric turbulence was first put forward by Kolmogorov (1941a,b). In these seminal works, Kolmogorov established fundamental properties of turbulence dynamics and energy transfer across turbulent scales through the use of velocity structure functions. The structure

functions and associated structure parameters for velocity are important for assessing boundary layer mixing (Moulsley et al. 1981), turbulence intermittency (Gaudin et al. 1998), and acoustic wave scattering (Little 1969).

In this paper, we extend the work of Gibbs et al. (2016), which dealt with structure functions of potential temperature fluctuations, and focus on second-order velocity structure functions and corresponding structure parameters in the atmospheric convective boundary layer (CBL). In Gibbs et al. (2016), three methods to compute the potential temperature structure parameter for two atmospheric CBL regimes were evaluated. Those methods included the *direct* method (DM), the *true spectral* method (TSM), and the *conventional spectral* method (CSM). Hereinafter, we modify the naming of the CSM to the *approximate spectral* method (ASM) for reasons discussed in section 2. The DM implies the evaluation of the structure function by directly applying its mathematical formulation to the gridded numerical simulation data. The structure parameter is then found by limiting the structure function to spatial increments that lie within the inertial subrange of turbulence scales. According to the TSM, the structure function is calculated through an integral relationship between the spectral density and second-order structure function under the assumption of turbulence isotropy. The computational burden of the TSM may be reduced as compared with the DM due to the numerical efficiency of the fast Fourier transform (FFT) technique used for computing spectra, although the numerical evaluation of the integral may offset such gains. The structure parameter is then retrieved from the structure function in the same manner as with the DM. Last, the ASM is based on an analytical relationship between the structure parameter and spectral density of velocity by assuming that the velocity spectrum follows the inertial-subrange scaling over the entire wavenumber range (from 0 to ∞). This simplification makes the ASM the least computationally intensive procedure and is the main

Corresponding author: Jeremy A. Gibbs, jeremy.gibbs@noaa.gov

reason for its popularity in practical evaluation of structure parameters, at least when applied to fluctuations of atmospheric scalars (e.g., Kaimal 1973; Wyngaard and LeMone 1980; Green et al. 1994; Cheinet and Siebesma 2009; Maronga 2014).

In Gibbs et al. (2016), potential temperature structure parameters evaluated by the DM and TSM were found to be nearly identical except, most notably, in the near-surface region, where turbulence anisotropy over horizontal planes manifests most strongly. Conversely, the potential temperature structure parameters computed according to the ASM were comparatively overpredicted by as much as an order of magnitude. It was hypothesized that this discrepancy was a result of assumptions underlying the ASM, and that such behavior was further exacerbated in regions prone to deviations from local isotropy. Accordingly, the DM and TSM were recommended as the preferred methods to evaluate structure parameters using gridded numerical simulation data.

In the current work, we use high-resolution large-eddy simulation (LES) to reproduce 3D velocity fields in a shear-free and a shear-driven atmospheric CBL. Turbulence properties are explored using velocity structure functions, and the velocity structure parameters are computed using the three methods summarized above, with comparisons made between results obtained by each method. Descriptions of the methods used to evaluate structure functions and structure parameters are given in section 2. Details of the numerical simulations and data processing methodology are presented in section 3. Results are shown in section 4, while discussion and conclusions are provided in section 5.

2. Structure function and structure parameter formulations

Spatial variability of velocity component fluctuations associated with atmospheric turbulence may be described in terms of the second-order velocity structure function (Tatarskii 1961; Pope 2000; Wyngaard 2010), given by the tensor

$$D_{ij}(\mathbf{r}) = \overline{[u_i(\mathbf{x}+\mathbf{r}) - u_i(\mathbf{x})][u_j(\mathbf{x}+\mathbf{r}) - u_j(\mathbf{x})]}, \qquad (1)$$

where $\mathbf{x}$ is the position vector, $\mathbf{r}$ is the separation vector, and u_i and u_j ($i = 1, 2, 3$; $j = 1, 2, 3$; $u_1, u_2, u_3 = u, v, w$) are velocity fluctuation components associated with the coordinate directions x_k ($k = 1, 2, 3$; $x_1, x_2 = x, y$: horizontal, $x_3 = z$: vertical). Here, $u_i = U_i - \overline{U_i}$, where U_i is the velocity component and overbars denote planar means. The consideration of individual components of the structure function is necessary since the velocity field is a vector (Obukhov and Yaglom 1959). Under the assumption that turbulence is locally isotropic and that the separation distance lies within the inertial subrange of spatial scales associated with turbulent velocity fluctuations (i.e., $r \equiv |\mathbf{r}| \ll \mathscr{L}$, where $\mathscr{L}$ is the characteristic length scale of the flow), then D_{ij} is an isotropic function of $\mathbf{r}$ that is independent of coordinate position (Pope 2000). Accordingly, D_{ij} is written

$$D_{ij}(\mathbf{r}) = D_{NN}(r)\delta_{ij} + [D_{LL}(r) - D_{NN}(r)]\frac{r_i r_j}{r^2}, \qquad (2)$$

where the scalar functions of separation distance D_{LL} and D_{NN} are referred to as the longitudinal and transverse structure

functions. If the coordinate system is oriented such that the separation vector is in the x direction (i.e., $\mathbf{r} = \mathbf{e}_1 r$), then

$$D_{11} = D_{LL}, \qquad (3a)$$

$$D_{22} = D_{33} = D_{NN}, \quad \text{and} \qquad (3b)$$

$$D_{ij} = 0 \quad \text{for} \quad i \neq j. \qquad (3c)$$

Based on the similarity hypotheses presented in Kolmogorov (1941a), the velocity structure function may be written as

$$D_{ij}(\mathbf{r}) = C_2 \varepsilon^{2/3} r^{2/3} \left(\frac{4}{3}\delta_{ij} - \frac{1}{3}\frac{r_i r_j}{r^2}\right) = C_{ij}^2 r^{2/3}, \qquad (4)$$

where C_2 is a universal constant, ε is the turbulence kinetic energy dissipation rate, and C_{ij}^2 is the velocity structure-function parameter, often called just the velocity structure parameter. Note that C_{ij}^2 is a constant and that the subscript is a reference to the order of the corresponding structure function and is not an indication of its tensor rank. According to (4),

$$C_{11}^2 = C_{LL}^2 = C_2 \varepsilon^{2/3}, \qquad (5a)$$

$$C_{22}^2 = C_{33}^2 = C_{NN}^2 = \frac{4}{3}C_2 \varepsilon^{2/3}, \quad \text{and} \qquad (5b)$$

$$C_{ij}^2 = 0 \quad \text{for} \quad i \neq j. \qquad (5c)$$

The longitudinal and transverse velocity structure parameters are related as $C_{NN}^2 = (4/3)C_{LL}^2$ based on (5). Consequently, $D_{NN} = (4/3)D_{LL}$ (Essenwanger and Reiter 1969; Pope 2000).

The velocity structure function may be directly computed using (1) applied to numerical LES gridded data if the turbulence is assumed to be isotropic, and ensemble averaging is approximated by evaluating means over statistically homogeneous spatial directions. Using such directly computed structure functions, the velocity structure parameter may be evaluated for a given separation distance by normalizing the inertial subrange value of D_{ij} by the corresponding inertial subrange separation distance r according to (4). We adopt the naming convention in Gibbs et al. (2016) and refer to this procedure as the direct method. As noted in Gibbs et al. (2016), this method has certain drawbacks despite its straightforwardness as compared to the other methods presented below. By design, the DM requires data on velocity from multiple locations within the flow. Furthermore, while this limitation may be overcome by applying Taylor's frozen turbulence hypothesis to high-frequency temporal data at a single location, the generalizability of the method is compromised when it is applied to heterogeneous atmospheric flows.

We explore two alternative methods discussed in Gibbs et al. (2016) based on the mathematical relationship between D_{ij} and one-dimensional spectral density of velocity Φ_{ij}. The designation of these methods is to evaluate the velocity structure parameter from simulation (and potentially, also observational) data in the most efficient manner while retaining as much of the original physical interpretation as possible. The first of the alternatives to the DM is called the true spectral method. It is based on the following relationship between D_{ij} and Φ_{ij}

under the assumption of turbulence isotropy (Tatarskii 1961; Wyngaard 2010):

$$D_{ij}(r) = 4 \int_0^\infty [1 - \cos(kr)]\Phi_{ij}(k)\,dk, \tag{6}$$

where $k \equiv |\mathbf{k}|$ is the wavenumber. The "true" part of the method name points to the lack of any assumption made about the form of the spectral density function Φ_{ij} in the integral. Using the TSM, D_{ij} is numerically computed from LES gridded data through (6) once Φ_{ij} is known. Employing the numerical FFT technique for calculation of the spectral function makes the TSM technique attractive compared to the numerical overhead associated with the DM, although potential gains may be offset by the combined effects of computing spectral density and the numerical evaluation of the integral in (6).

The second alternative to the DM considered in Gibbs et al. (2016) is what we call the approximate spectral method, which is referred to by Gibbs et al. (2016) as the conventional spectral method. However, to our knowledge, this method is not as widely reported in the literature for velocity as for refractive index and temperature, which makes the term "conventional" potentially misleading in this context. According to ASM, the integral in (6) is evaluated analytically for Φ_{ij} assumed to have the inertial-subrange representation $\Phi_{ij} = Ak^{-5/3}$ across the entire range of turbulence scales (Tatarskii 1961; Essenwanger and Reiter 1969; Wyngaard et al. 1971), that is, for k from 0 to ∞, which provides

$$4 \int_0^\infty [1 - \cos(kr)]\Phi_{ij}(k)\,dk = 4A \int_0^\infty [1 - \cos(kr)]k^{-5/3}\,dk$$
$$= \frac{2\pi A r^{2/3}}{\Gamma(5/3)\sin(\pi/3)},$$

where Γ is the gamma function. Making use of (4) yields

$$\frac{2\pi A r^{2/3}}{\Gamma(5/3)\sin(\pi/3)} = C_{ij}^2 r^{2/3}.$$

Solving for A provides

$$A = \frac{C_{ij}^2 \Gamma(5/3)\sin(\pi/3)}{2\pi} \approx 0.125 C_{ij}^2, \tag{7}$$

which results in

$$\Phi_{ij} = Ak^{-5/3} = 0.125 C_{ij}^2 k^{-5/3}. \tag{8}$$

Rearranging (8) leads to the following approximate relationship between the velocity structure parameter and velocity spectrum:

$$C_{ij}^2 \approx \frac{\Phi_{ij}(k)}{0.125 k^{-5/3}}. \tag{9}$$

The value 0.125 in the denominator of (9) differs from the widely adopted proportionality coefficient of 0.25 originally presented in Wyngaard et al. (1971). We refer the reader to Gibbs and Fedorovich (2020) for a formal derivation that shows the value of 0.25 is an error. The ASM is advantageous computationally since the estimation of C_{ij}^2 only requires evaluation of Φ_{ij} within the inertial subrange. Separately, the ASM may be applied to point observations using instruments with fast sensors, which makes it attractive experimentally since these sensors produce spectra that are less susceptible to deviations from Kolmogorov's behavior due to their ability to sample turbulence on the smallest observable scales.

3. Experimental design

a. Numerical simulation code

Two simulations were conducted using MicroHH (van Heerwaarden et al. 2017), an open-source computational fluid dynamics code, applied in LES mode. The code has proven successful at faithfully reproducing atmospheric flows across a range of environmental regimes (e.g., van Heerwaarden et al. 2014; Gentine et al. 2015; Fedorovich et al. 2017; van der Linden et al. 2019). The filtered Boussinesq-approximated Navier–Stokes equations of motion and scalar transport equations are spatially discretized and solved numerically using second-order, centered finite differencing of the advection and diffusion terms. A third-order Runge–Kutta scheme is applied for time integration of these equations, and a second-order Poisson solver is used for pressure. The subgrid turbulence closure is based on the Lilly–Smagorinsky model (Lilly 1967), in which the subfilter eddy diffusivity is assumed proportional to the strain-rate tensor and the subfilter scalar diffusivity is prescribed using the subgrid turbulent Prandtl number.

b. Simulated convective boundary layers

We applied the three methods described in section 2 (DM, TSM, and ASM) to gridded numerical output from LES of a shear-free (hereinafter "Free") and shear-driven (hereinafter "Shear") CBL. The studied CBL flow types were qualitatively similar to those reproduced by the University of Oklahoma LES (OU-LES) code used in Gibbs et al. (2016). One difference is enhanced spatial resolution in our current simulations. Another difference is that we now operate with buoyancy instead of potential temperature. The buoyancy is defined through $b = g(\Theta - \Theta_{\text{env}})/\Theta_r$, where g is acceleration due to gravity, Θ is potential temperature, Θ_{env} is the environmental potential temperature, and Θ_r is a constant reference potential temperature.

Configuration details for each simulation are provided in Table 1. Each simulation was initialized with a vertically constant statically stable background stratification quantified in terms of N^2, where $N = [(g/\Theta_r)(d\Theta_{\text{env}}/dz)]^{1/2}$ is the Brunt–Väisälä frequency. The Coriolis parameter was set with consideration to midlatitudes in the Northern Hemisphere. The lower and upper boundary conditions for velocity were no-slip and free-slip, respectively. The corresponding conditions for buoyancy were prescribed in the form of buoyancy flux, positive at the lower boundary and zero at the top boundary. Lateral boundary conditions for all prognostic fields were periodic. A Rayleigh damping layer was applied in the upper 20% of the domain. A constant geostrophic wind $u_g = 10\,\text{m s}^{-1}$ was

TABLE 1. Simulation configuration values for geostrophic wind u_g ($v_g = 0$), background stratification N^2, surface kinematic buoyancy flux $\overline{w'b'}$, Coriolis parameter f_c, surface roughness z_0 (equal for momentum and scalars), grid spacing Δ, and numerical mesh size $N_x \times N_y \times N_z$.

Case	u_g (m s^{-1})	N^2 (s^{-2})	$\overline{w'b'}$ (m^2 s^{-3})	f_c (s^{-1})	z_0 (m)	Δ (m)	$N_x \times N_y \times N_z$
Free	0	10^{-4}	4×10^{-3}	10^{-4}	0.10	4	$1024 \times 1024 \times 512$
Shear	10						

applied in the x direction in the Shear case, and u_g was set to zero in the Free case.

Properties of each simulation are given in Table 2. Each simulation was run for approximately 30 large-eddy turnover times $T_* = z_i/w_*$ (6 h of physical time), where z_i is the boundary layer depth (computed as the level at which the vertical buoyancy flux $\overline{w'b'}$ reaches its minimum negative value) and $w_* = (z_i \overline{w'b'_s})^{1/3}$ is the convective velocity scale (Deardorff 1972), where subscript s indicates the surface value. The three velocity component fields were extracted after the fourth hour ($\approx 22T_*$). This time frame was selected because the CBL was fully developed and its top ($z_i = 1030$ m in the Free case and $z_i = 1126$ m in the Shear case) did not unduly impinge on the damping layer at the top of the simulation domain. Additional parameters describing each simulation are also given in Table 2, including friction velocity $u_* = (\overline{u'w'_s}^2 + \overline{v'w'_s}^2)^{1/4}$, buoyancy scale $b_* = -\overline{w'b'_s}/u_*$, Obukhov length $L = u_*^2/(\kappa b_*)$, and instability parameter $-z_i/L$.

Potential temperature deviations from means over horizontal planes are shown in Fig. 1, which allow for visualization of dominant CBL flow structures for each regime over vertical and horizontal cross sections of the flow. Potential temperature deviation $\theta = \Theta - \Theta_r$ is related to buoyancy as $\theta = (\Theta_r/g)[b - N^2(L_z - z)]$, where Θ_r is set to 300 K and L_z is the domain length in the vertical direction. The Free CBL displays the expected organized cellular-type convection with vertically oriented structure (e.g., Deardorff 1972; Schmidt and Schumann 1989; Sullivan and Patton 2011), while the Shear CBL shows evidence of elongated flow-aligned rolls that are rotated horizontally due to the joint effect of the Coriolis force and turbulent friction, and tilted vertically due to mean wind shear (e.g., Moeng and Sullivan 1994; Khanna and Brasseur 1998; Salesky et al. 2017).

c. Data processing

Before computing the structure functions and spectra, horizontal planar means (denoted by overbars) were subtracted from each field to produce perturbation quantities $u_i = U_i - \overline{U_i}$. We follow the procedures outlined in Gibbs et al. (2016) for each method used to compute the structure parameters for velocity.

Let us consider the DM, which implies direct evaluation of the velocity structure function. We choose a coordinate system where the separation vector is in the x direction ($\mathbf{r} = \mathbf{e}_1 r$). As described in (3), D_{ij} is only defined for $i = j = 1, 2, 3$ under this alignment. Accordingly, we start by summing the square differences of each velocity component in the x direction at a given height and for a given separation distance using (1) {i.e., summing $[u_i(x + r, y, z) - u_i(x, y, z)]^2$}. The sum is only modified if $x + r \le L_x$, where L_x is the domain length in the x direction. Last, we divide the sum by the number of incremental squared differences to arrive at the structure function $D_{ij}(z, r)$. This process is repeated for all separation distances and vertical levels. We separately repeated this process for a separation vector oriented in the y direction ($\mathbf{r} = \mathbf{e}_2 r$) and found results to be consistent with the change of separation vector orientation (not shown). Additionally, Wilson and Fedorovich (2012) describe a procedure to compute the structure function through separations in the z direction ($\mathbf{r} = \mathbf{e}_3 r$), where the squared differences for a particular separation distance are evaluated as the averages of the differences in the positive (upward) and negative (downward) directions. However, the number of physically meaningful separation distances is severely limited near the upper and lower boundaries when using this procedure. These flow regions, especially the one near the lower boundary, are also prone to anisotropy and non-Kolmogorov turbulence spectral behavior. This affects the robustness and interpretability of computed structure functions. For these reasons, we only consider structure functions based on separations in the x direction.

Spectral densities (spectra) of velocity components are needed for both the TSM and ASM. Consistent with Gibbs et al. (2016), we followed the spectrum computation algorithm described in Gibbs and Fedorovich (2014). For a given horizontal plane, spectral density was computed for each velocity component in the x direction (Φ_{11}, Φ_{22}, Φ_{33}) and then averaged in the y direction. This process was repeated for each vertical level. For the TSM, the structure function was computed at each height and for all separation distances using (6). Next, the inertial subrange values of r (r_{isr}) and k (k_{isr}) need to be evaluated in order to compute the structure parameters for each method.

TABLE 2. Simulation properties, including boundary layer depth z_i, Obukhov length L, instability parameter $-z_i/L$, friction velocity u_*, buoyancy scale b_*, and convective velocity scale w_* at the comparison time of 14 400 s.

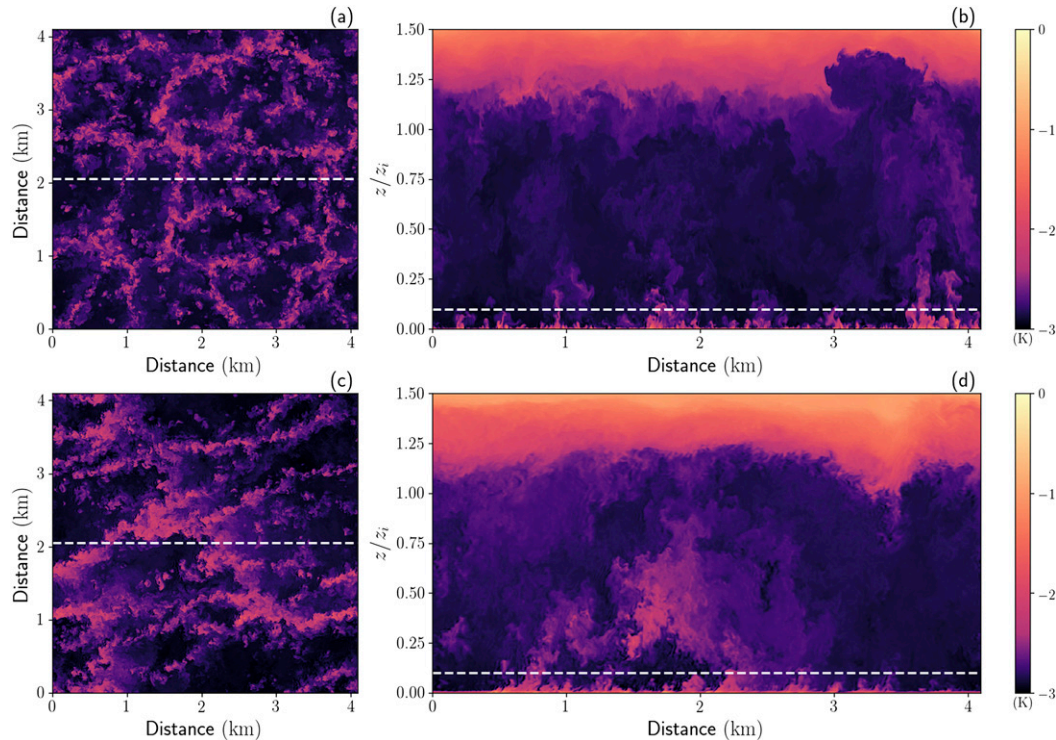| Case	z_i (m)	L (m)	$-z_i/L$	u_* (m s^{-1})	b_* (m s^{-2})	w_* (m s^{-1})
Free	1030	-3.42	301.42	0.18	-0.023	1.60
Shear	1126	-74.97	15.02	0.50	-0.008	1.65

FIG. 1. Potential temperature perturbations reproduced by MicroHH for the (a),(b) Free case and (c),(d) Shear case. (left) Horizontal x–y cross sections are taken at $z/z_i = 0.1$, where z_i is the depth of the boundary layer, and (right) x–z vertical cross sections are taken at the midpoint in the y direction. Cross-sectional locations are denoted by dashed white lines.

We first attempted an objective method (hereinafter the polyfit method) very similar to that used in Gibbs et al. (2016), which itself was based on a method suggested by Hartogensis and De Bruin (2005). At each height, a polynomial regression was fit to the spectra since the raw spectra were very noisy locally in wavenumber space. Before doing so, we cut structure functions and spectra over the 100 largest wavenumbers. These large wavenumber parts are practically never within the inertial subrange, and their absence from the regression calculation does not affect the identification thereof. Using the regression line, the inertial subrange was established objectively as the widest contiguous region of wavenumbers over which the slope in logarithmic space followed the $-5/3$ power law within a 20% error tolerance. An analogous procedure was used to determine the inertial subrange for structure functions by applying the 2/3 power-law criterion to the logarithmic slope. The geometric means of r and k within the identified subranges were taken to compute r_{isr} and k_{isr}. If the identified inertial subrange extended over fewer than three wavenumbers (separation distances), then that vertical level was ignored. At the end of the procedure, missing values were computed via interpolation. We found this method to be very sensitive to the choice of regression, error tolerance, and smoothing filter applied to the data. Such issues with ad hoc methods are well known (Ortiz-Suslow et al. 2020).

We next sought a more robust objective method that required far less human intervention. We rescaled structure functions and spectral densities by multiplying D_{ij} by $r^{-2/3} z_i^{2/3} w_*^{-2}$ and Φ_{ij} by $k^{5/3} z_i^{2/3} w_*^{-2}$. In doing so, the structure functions and spectral densities associated with the inertial subrange are within some measure of a flat plateau range, while the values outside of the inertial subrange range decrease from both sides of this plateau. Accordingly, we call this the flattop method, which is similar to procedures applied to previous channel flow simulations (Jabbari et al. 2015). Rescaled spectral densities were additionally subjected to a median-type smoother to remove the effects of local noise. Last, the values for r_{isr} and k_{isr} were found by locating the maximum value of the rescaled data. The maximum acts as an inflection point within the inertial subrange and is thus a proxy for the geometric mean value found using the polyfit method. Vertical changes of r_{isr} and k_{isr}, along with the associated structure functions and spectral densities, are shown in Figs. 2 and 3. Values between the polyfit and flattop methods were statistically similar. Due to the lack of human intervention, we chose the flattop method since it is easier in practical implementation without undermining physical interpretability.

Last, the r_{isr} identified by the flattop method and the structure function associated with r_{isr} were applied using (4) to compute the structure parameters according to the DM and TSM. The structure parameter according to the ASM was found at each height by applying the flattop procedure to the relevant spectra to identify k_{isr}, which were then used in (9). Standard error values were very small compared with the structure parameter at each height due to a large effective
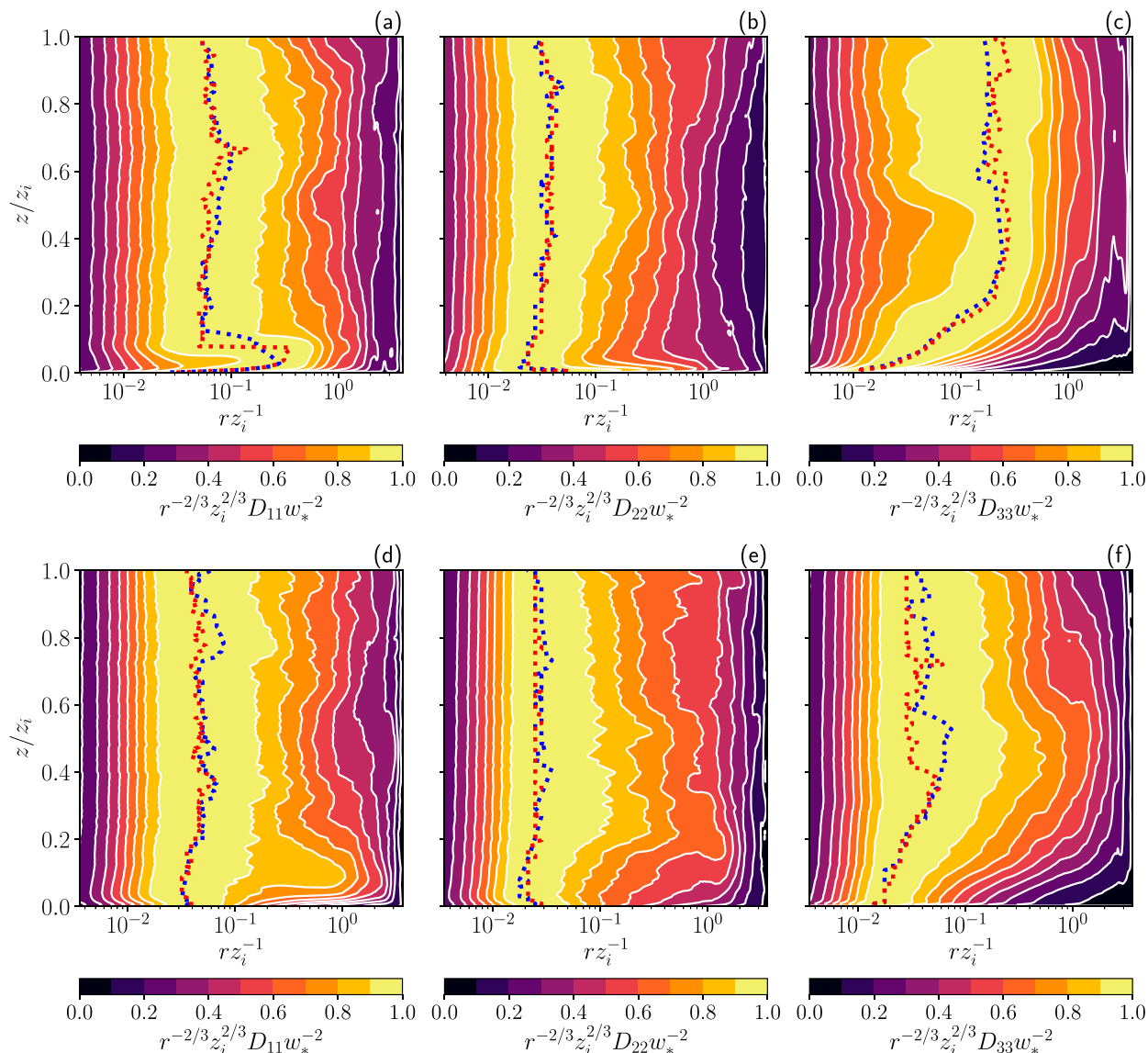
FIG. 2. Rescaled structure functions of velocity for the (a)–(c) Free case and (d)–(f) Shear case. Values are normalized by the local (in height) maxima. The values of r_{isr} found using the polyfit (blue dotted line) and flattop (red dotted line) methods are shown.

sample size. Thus, the corresponding confidence intervals are not shown in the respective figures.

4. Results

Here we present both structure functions and structure parameters for velocity components computed using the methods outlined in section 3c.

a. Structure functions

To evaluate representative turbulence characteristics of the considered CBL flow types, we first examine the structure functions computed using the DM. The longitudinal and transverse structure functions, as well as the theoretical relationship between the two, are shown in Fig. 4 as functions of separation distance at height $z/z_i = 0.5$. The transverse

structure function values are larger than those of the longitudinal counterparts for horizontal flow components, as expected, in both the Free and Shear cases. In the Free case, the inertial subrange is identified as the range of scales where D_{11} and D_{22} follow closely the 2/3 power-law slope. This region is approximately coincident with, and slightly wider than, the range of scales where the local isotropy relationship $D_{22} = (4/3)D_{11}$ holds (Pope 2000). On the other hand, D_{33} has a much narrower inertial subrange and its values are noticeably larger than $(4/3)D_{11}$. Additionally, the D_{33} slope actually increases at larger separations ($r \approx 0.1$–$0.6z_i$). We suspect that this feature reflects the cellular convection organization of the CBL flow, where the narrow bands of updrafts cause the slopes of structure functions to steepen. Visual inspection of Fig. 1 indicates that the
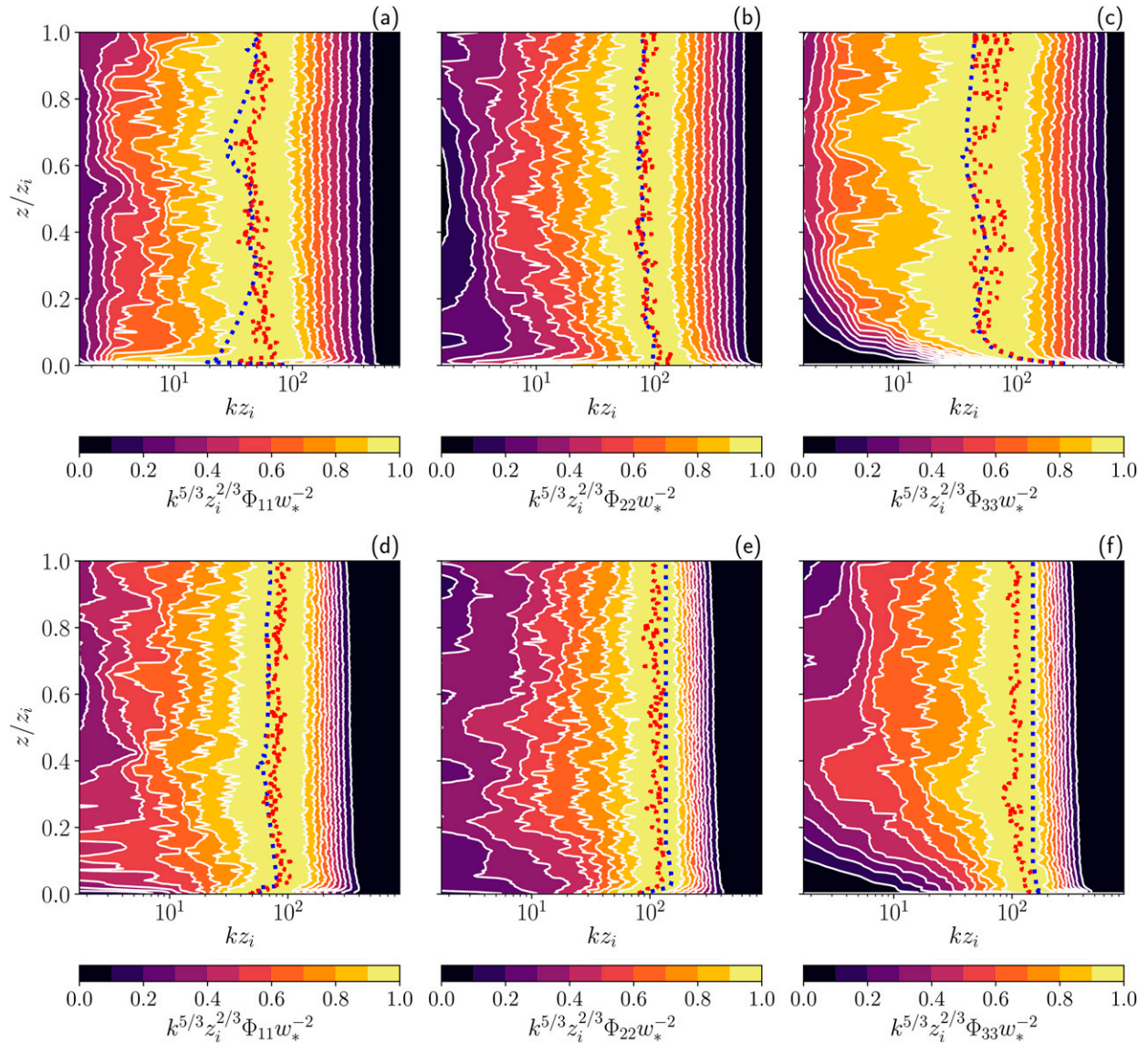
FIG. 3. Rescaled one-dimensional spectral density of velocity for the (a)–(c) Free case and (d)–(f) Shear case. Values are normalized by the local (in height) maxima. The values of k_{isr} found using the polyfit (blue dotted line) and flattop (red dotted line) methods are shown.

characteristic spacing between these bands is roughly within the range of increased slope. A more detailed objective measure of these effects is needed, however, and is beyond the scope of the current work. One potential future avenue is to explore the "roll factor" introduced in Salesky et al. (2017), which is based on the two-point correlation of vertical velocity in polar coordinates across horizontal planes. In the Shear case, there is again a range of scales, albeit narrower than in the Free case, where the 2/3 power law and local isotropy hold for D_{11} and D_{22}. In contrast, D_{33} follows the 2/3 power-law slope for a range scales in the Shear case and its value does not exceed $(4/3)D_{11}$ by as much as it does in the Free case. Apparently, assumptions of local isotropy for D_{33} are better upheld in boundary layers with the presence of mean shear than in those without.

b. Structure-function parameters

We now show and discuss the structure parameters for velocity components. First, we will examine turbulence isotropy by comparing longitudinal and transverse structure parameters. Next, we compare profiles of the structure parameters as computed by the DM, TSM, and ASM.

1) LONGITUDINAL VERSUS TRANSVERSE

Vertical profiles of normalized C_{ij}^2 values computed using the DM are presented in Fig. 5. The first notable feature is that the structure parameters are enhanced near the surface in the Shear case as compared with those in the Free case. Above the boundary layer, the relationship is reversed and the values in the Shear case are smaller than those in the Free case. The former feature is likely due to enhanced variability caused by
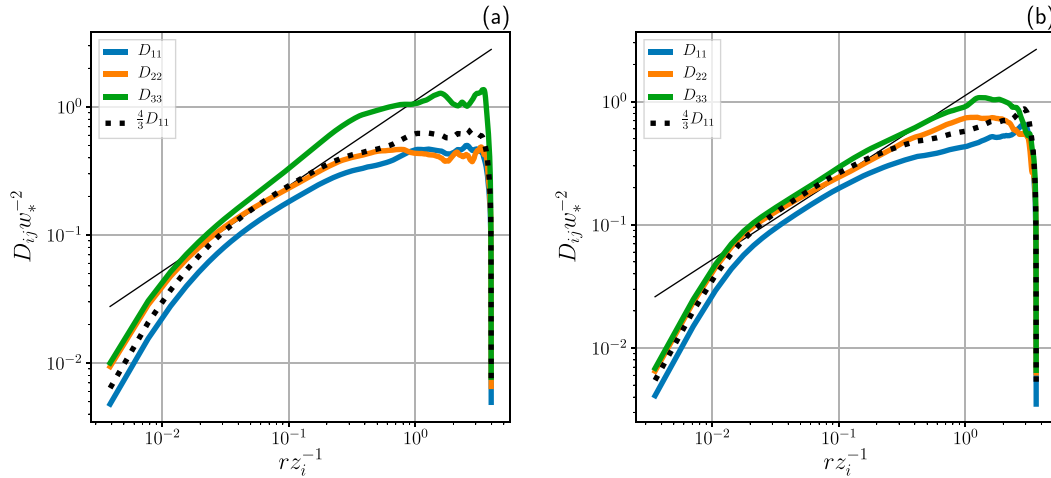
FIG. 4. Structure functions of velocity computed using the DM for the (a) Free and (b) Shear cases. Solid black lines represent the theoretical 2/3 power law.

surface shear, while the latter is perhaps related to entrainment effects specific to sheared CBLs. In both the Free and Shear cases, the transverse parameters are larger than the longitudinal parameters throughout most of the boundary layer, except in the surface layer ($z \lesssim 0.1z_i$) where they reverse position. Another way to view this feature is through the theoretical relationship between the longitudinal and transverse structure parameters $[C_{NN}^2 = (4/3)C_{LL}^2]$. In both cases, there is a fairly deep range of heights over which the assumption of local isotropy holds for C_{11}^2 and C_{22}^2, consistent with results discussed in section 4a. There is a notable divergence above the top of the boundary layer and in the lower portion of the domain that maximizes near the surface. The level near the surface where $C_{22}^2 \neq (4/3)C_{11}^2$ may signify the lower bounds of the well-mixed boundary layer, while the departure near the top of the profiles may serve as an identifier for the entrainment layer. The agreement between C_{11}^2

and C_{22}^2 with theory throughout the depth of the CBL does not imply that the flow is substantially isotropic. Rather, it simply illustrates that there exists a range of separation distances at each height where the flow is locally isotropic. In the Free case, there is no agreement with local isotropy prediction for C_{33}^2 at any height, which means that our implicit assumption of local isotropy over horizontal planes is violated for vertical velocity. The same is partly true in the Shear case, although the vertical profile of C_{33}^2 is much closer in value to $(4/3)C_{11}^2$ and more closely follows its slope over a major portion of the CBL depth. Apparently, the existence of organized cellular structures and, to a lesser extent, roll-like structures means that the associated inertial subranges of vertical velocity are very narrow if they exist at all. Consequently, the structure parameter only describes turbulence over a very constrained range of scales, which minimizes its utility in flows (or flow regions) where the 4/3
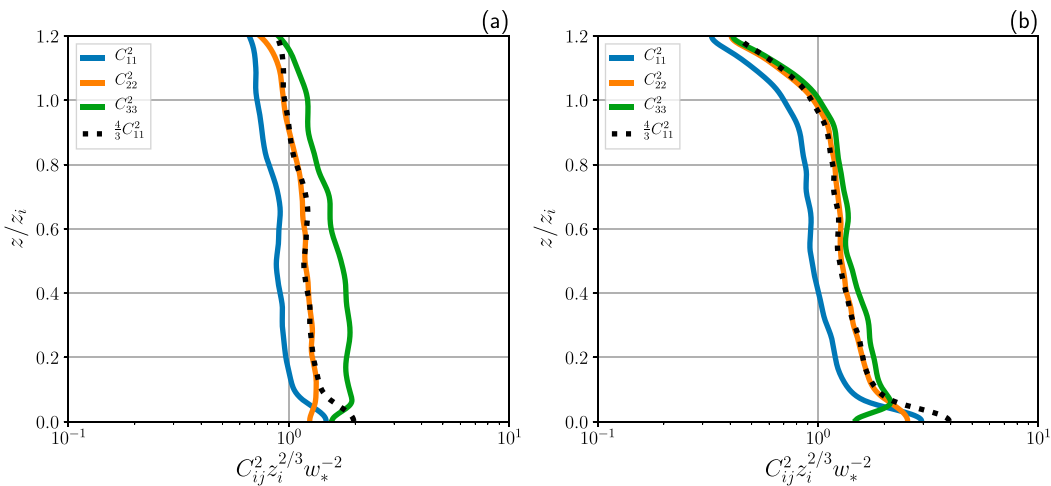

FIG. 5. Structure-function parameters of velocity computed using the DM for the (a) Free and (b) Shear cases. Dashed black lines are the theoretical isotropic transverse structure parameter defined by $C_{NN}^2 = (4/3)C_{LL}^2$.
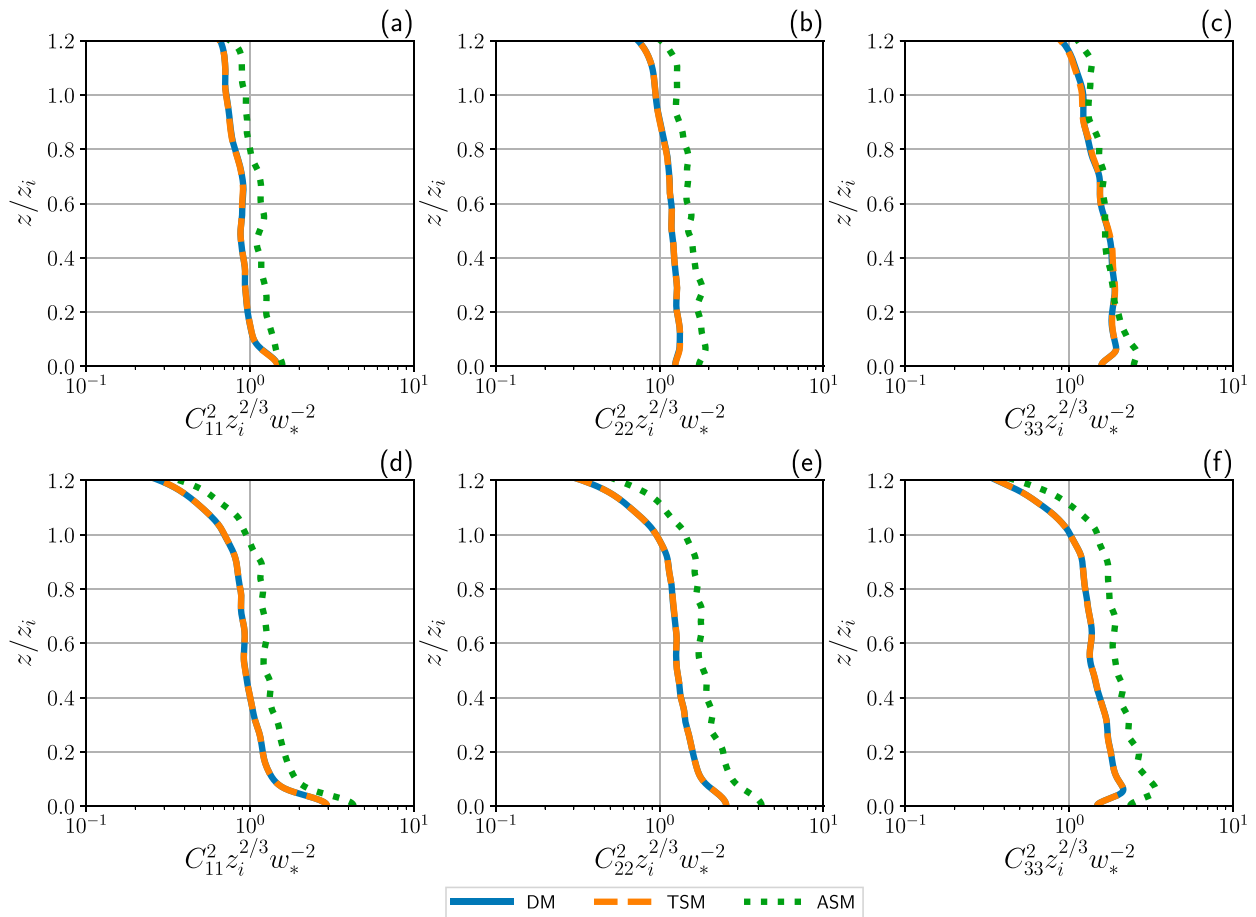
FIG. 6. Structure-function parameters of velocity computed using the DM (blue solid lines), TSM (orange dashed lines), and ASM (green dotted lines) for the (a)–(c) Free case and (d)–(f) Shear case.

relationship no longer holds due to anisotropy and departures from the Kolmogorov spectrum.

2) DIRECT VERSUS SPECTRAL METHODS

Last, we compare vertical profiles of C_{ij}^2 as computed by the DM, TSM, and ASM in Fig. 6. In all cases and for all velocity components, structure parameters computed according to the DM and TSM are practically identical. This outcome is expected since these two methods are mathematically equivalent Tatarskii (1961). Conversely, and consistent with findings in Maronga et al. (2014) and Gibbs et al. (2016), the ASM overestimates the structure parameter as computed by the other two methods at each level by nearly as much as a factor of 2. The overestimation by the ASM is smallest for D_{33} in the Free case, where the increased spectral energy (variance) associated with persistent cellular convection masks the failure of the inherent assumptions of this method that the entire spectrum follows inertial subrange scaling ($-5/3$ power law).

5. Discussion and conclusions

In this paper, we focus on structure functions and structure parameters for velocity fields in two CBL types (Free and Shear). Atmospheric boundary layer literature has historically paid less attention to these velocity functions/parameters in favor of their scalar counterparts (temperature, moisture, refractive index), despite the utility of the former to assess boundary layer mixing, turbulence intermittency, acoustic wave scattering, and more. We demonstrated the feasibility of direct retrieval of the velocity structure functions and parameters from numerically simulated CBL flow fields. Three methods were compared: calculating the structure function and parameter directly according to their mathematical definitions (DM), computing the same quantities using an integral relationship between the structure function and spectral density of velocity (TSM), and employing an analytical approximation of the TSM that relates the structure parameter to spectral density in the inertial subrange (ASM).

In both the Free and Shear cases, the structure functions for horizontal velocity components exhibited extended regions that followed the 2/3 power law in the middle section of the CBL (at $z/z_i = 0.5$). The lower limit of this range was approximately 4–5 times the grid spacing used in the numerical LES mesh, which matches the findings of

Wilson and Fedorovich (2012). Additionally, assumptions of local isotropy $[D_{22} = (4/3)D_{11}]$ were verified over a range of separation distances. The inertial subrange according to the 2/3 power law in the structure function for vertical velocity was rather narrow in the Free case, with D_{33} exhibiting a steepening slope at larger separation distances. We hypothesize that this is a result of organized cellular convection structure in the flow. Conversely, the inertial subrange for D_{33} was wider in the Shear case. In both cases, the assumption of local isotropy $[D_{33} = (4/3)D_{11}]$ was violated, although the effect was less substantial in the Shear case.

Vertical profiles of the associated structure parameters indicated that values were enhanced (reduced) near the surface (boundary layer top) in the presence of shear. Profiles also demonstrated that local isotropy was upheld for C_{11}^2 and C_{22}^2 through an extended range of heights within the boundary layer in both cases. Exceptions to this agreement were notable near the surface and at the top of the boundary layer, coincident with anisotropy effects caused by the lower surface and entrainment, respectively. Vertical profiles of C_{33}^2 showed no compliance with local isotropy at any level in the Free case. This behavior suggests that the entire concept of structure parameters for fluctuations of the vertical velocity in shear-free CBLs appears to be nonapplicable due to the existence of persistent cellular structures in these flow regimes. Alternatively, C_{33}^2 in the Shear case closely followed the slope of $(4/3)C_{11}^2$ throughout a large portion of the CBL depth, although its magnitude still remained too large. It is possible, based on the instability parameter given in Table 2, that the Shear case presented here is within the hybrid regime described in Salesky et al. (2017), where both rolls and cellular structures coexist. Future studies should examine whether the assumptions of local isotropy, and thus the efficacy of structure parameters, are improved for vertical velocity as the flow becomes more weakly convective and shear-driven.

Vertical profiles of the structure parameters as computed by the DM, TSM, and ASM were compared across cases. In all situations, the DM and TSM were nearly identical. Meanwhile, the ASM overestimated these values for all scenarios by a factor of up to 2. Note that (6) places no limits on the velocity spectrum, while (9) assumes that the entire velocity spectrum follows inertial subrange scaling. In other words, the TSM allows for regions of the spectral density beyond the inertial subrange, while the ASM does not. Consider the idealized spectra in Fig. 7, where a comparison is presented of the Kolmogorov spectrum with a spectrum from a typical large-eddy simulation. The integral of the former is notably larger than of the latter. The result is an apparent overestimation of C_{ij}^2. This interpretation matches the analysis presented in Gibbs et al. (2016). It is important to note, however, that the level of exaggeration is likely reduced when applied to aircraft and large-aperture scintillometer data (Braam et al. 2016). On the other hand, the level of agreement in most of the reported observational studies is likely overstated, since they use the incorrect constant of proportionality in the TSM (0.25 instead of 0.125). The disparity between numerical and observational agreement lies in the fact that the fast sensors used to collect
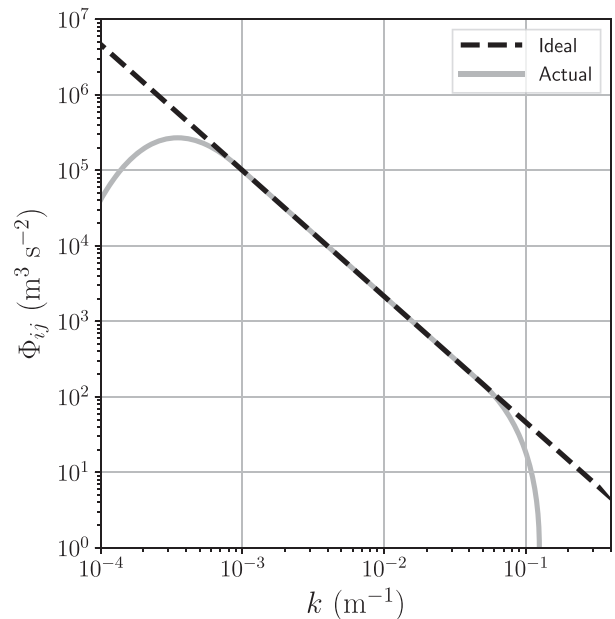

FIG. 7. Idealized velocity spectra. The black line follows Kolmogorov scaling across all wavenumbers, and the gray line is qualitatively representative of velocity spectra in the atmospheric boundary layer.

atmospheric data are able to better capture turbulence features within relatively broader inertial subranges than do LES codes. In accordance with Gibbs et al. (2016), we also suggest the use of either the DM or TSM when extracting the structure parameters for velocity from gridded numerical simulation output.

REFERENCES

Andreas, E. L., 1988: Estimating C_n^2 over snow and sea ice from meteorological data. *J. Opt. Soc. Amer.*, **5A**, 481–495, https://doi.org/10.1364/JOSAA.5.000481.

Braam, M., F. Beyrich, J. Bange, A. Platis, S. Martin, B. Maronga, and A. F. Moene, 2016: On the discrepancy in simultaneous observations of the structure parameter of temperature using scintillometers and unmanned aircraft. *Bound.-Layer Meteor.*, **158**, 257–283, https://doi.org/10.1007/s10546-015-0086-9.

Burk, S. D., 1980: Refractive index structure parameters: Time-dependent calculations using a numerical boundary-layer model. *J. Appl. Meteor.*, **19**, 562–576, https://doi.org/10.1175/1520-0450(1980)019<0562:RISPTD>2.0.CO;2.

Cheinet, S., and A. P. Siebesma, 2009: Variability of local structure parameters in the convective boundary layer. *J. Atmos. Sci.*, **66**, 1002–1017, https://doi.org/10.1175/2008JAS2790.1.

Deardorff, J. W., 1972: Numerical investigation of neutral and unstable planetary boundary layers. *J. Atmos. Sci.*, **29**, 91–115, https://doi.org/10.1175/1520-0469(1972)029<0091:NIONAU>2.0.CO;2.

Essenwanger, O., and E. R. Reiter, 1969: Power spectrum, structure function, vertical wind shear, and turbulence in troposphere and stratosphere. *Arch. Meteor. Geophys. Bioklimatol.*, **18A**, 17–24, https://doi.org/10.1007/bf02247861.

Fedorovich, E., J. A. Gibbs, and A. Shapiro, 2017: Numerical study of nocturnal low-level jets over gently sloping terrain. *J. Atmos. Sci.*, **74**, 2813–2834, https://doi.org/10.1175/JAS-D-17-0013.1.

Frederickson, P. A., K. L. Davidson, C. R. Zeisse, and C. S. Bendall, 2000: Estimating the refractive index structure parameter over the ocean using bulk methods. *J. Appl. Meteor.*, **39**, 1770–1783, https://doi.org/10.1175/1520-0450-39.10.1770.

Gaudin, E., B. Protas, S. Goujon-Durand, J. Wojciechowski, and J. E. Wesfreid, 1998: Spatial properties of velocity structure functions in turbulent wake flows. *Phys. Rev.*, **57E**, R9–R12, https://doi.org/10.1103/physreve.57.r9.

Gentine, P., G. Bellon, and C. C. van Heerwaarden, 2015: A closer look at boundary layer inversion in large-eddy simulations and bulk models: Buoyancy-driven case. *J. Atmos. Sci.*, **72**, 728–749, https://doi.org/10.1175/JAS-D-13-0377.1.

Gibbs, J. A., and E. Fedorovich, 2014: Comparison of convective boundary layer velocity spectra retrieved from large-eddy-simulation and Weather Research and Forecasting Model data. *J. Appl. Meteor. Climatol.*, **53**, 377–394, https://doi.org/10.1175/JAMC-D-13-033.1.

——, and ——, 2020: On the evaluation of the proportionality coefficient between the turbulence temperature spectrum and structure parameter. *J. Atmos. Sci.*, **77**, 2761–2763, https://doi.org/10.1175/jas-d-19-0344.1.

——, ——, B. Maronga, C. Wainwright, and M. Dröse, 2016: Comparison of direct and spectral methods for evaluation of the temperature structure parameter in numerically simulated convective boundary layer flows. *Mon. Wea. Rev.*, **144**, 2205–2214, https://doi.org/10.1175/MWR-D-15-0390.1.

Green, A. E., K. J. McAneney, and M. S. Astill, 1994: Surface-layer scintillation measurements of daytime sensible heat and momentum fluxes. *Bound.-Layer Meteor.*, **68**, 357–373, https://doi.org/10.1007/BF00706796.

Hartogensis, O. K., and H. A. R. De Bruin, 2005: Monin–Obukhov similarity functions of the structure parameter of temperature and turbulent kinetic energy dissipation rate in the stable boundary layer. *Bound.-Layer Meteor.*, **116**, 253–276, https://doi.org/10.1007/s10546-004-2817-1.

Jabbari, A., L. Boegman, and U. Piomelli, 2015: Evaluation of the inertial dissipation method within boundary layers using numerical simulations. *Geophys. Res. Lett.*, **42**, 1504–1511, https://doi.org/10.1002/2015GL063147.

Kaimal, J. C., 1973: Turbulence spectra, length scales and structure parameters in the stable surface layer. *Bound.-Layer Meteor.*, **4**, 289–309, https://doi.org/10.1007/BF02265239.

Khanna, S., and J. G. Brasseur, 1998: Three-dimensional buoyancy- and shear-induced local structure of the atmospheric boundary layer. *J. Atmos. Sci.*, **55**, 710–743, https://doi.org/10.1175/1520-0469(1998)055<0710:TDBASI>2.0.CO;2.

Kolmogorov, A. N., 1941a: The local structure of turbulence in incompressible viscous fluid for very large Reynolds numbers. *Dokl. Akad. Nauk SSSR*, **30**, 301–305.

——, 1941b: Dissipation of energy in the locally isotropic turbulence. *Dokl. Akad. Nauk SSSR*, **32**, 19–21.

Lesieur, M., and O. Metais, 1996: New trends in large-eddy simulations of turbulence. *Annu. Rev. Fluid Mech.*, **28**, 45–82, https://doi.org/10.1146/annurev.fl.28.010196.000401.

Lilly, D. K., 1967: The representation of small-scale turbulence in numerical simulations. *Proc. IBM Scientific Computing Symp. on Environmental Sciences*, Yorktown Heights, NY, IBM, 195–209.

Little, C. G., 1969: Acoustic methods for the remote probing of the lower atmosphere. *Proc. IEEE*, **57**, 571–578, https://doi.org/10.1109/PROC.1969.7010.

Maronga, B., 2014: Monin–Obukhov similarity functions for the structure parameters of temperature and humidity in the unstable surface layer: Results from high-resolution large-eddy simulations. *J. Atmos. Sci.*, **71**, 716–733, https://doi.org/10.1175/JAS-D-13-0135.1.

——, O. Hartogensis, S. Raasch, and F. Beyrich, 2014: The effect of surface heterogeneity on the structure parameters of temperature and specific humidity: A large-eddy simulation case study for the LITFASS-2003 experiment. *Bound.-Layer Meteor.*, **153**, 441–470, https://doi.org/10.1007/s10546-014-9955-x.

Moeng, C.-H., and P. P. Sullivan, 1994: A comparison of shear- and buoyancy-driven planetary boundary layer flows. *J. Atmos. Sci.*, **51**, 999–1022, https://doi.org/10.1175/1520-0469(1994)051<0999:ACOSAB>2.0.CO;2.

Moulsley, T. J., D. N. Asimakopoulos, R. S. Cole, B. A. Crease, and S. J. Caughey, 1981: Measurement of boundary layer structure parameter profiles by acoustic sounding and comparison with direct measurements. *Quart. J. Roy. Meteor. Soc.*, **107**, 203–230, https://doi.org/10.1002/qj.49710745113.

Obukhov, A. M., and A. M. Yaglom, 1959: On the microstructure of atmospheric turbulence—A review of recent work in the U.S.S.R. *Quart. J. Roy. Meteor. Soc.*, **85**, 81–90, https://doi.org/10.1002/qj.49708536402.

Ortiz-Suslow, D. G., Q. Wang, J. Kalogiros, and R. Yamaguchi, 2020: A method for identifying Kolmogorov's inertial subrange in the velocity variance spectrum. *J. Atmos. Oceanic Technol.*, **37**, 85–102, https://doi.org/10.1175/JTECH-D-19-0028.1.

Peltier, L. J., and J. C. Wyngaard, 1995: Structure–function parameters in the convective boundary layer from large-eddy simulation. *J. Atmos. Sci.*, **52**, 3641–3660, https://doi.org/10.1175/1520-0469(1995)052<3641:SPITCB>2.0.CO;2.

Pope, S. B., 2000: *Turbulent Flows*. Cambridge University Press, 771 pp.

Rizza, U., C. Mangia, J. C. Carvalho, and D. Anfossi, 2006: Estimation of the Lagrangian velocity structure function constant C_0 by large-eddy simulation. *Bound.-Layer Meteor.*, **120**, 25–37, https://doi.org/10.1007/s10546-005-9039-z.

——, G. A. Degrazia, C. Mangia, and E. P. M. Filho, 2010: Estimation of the Kolmogorov constant for the Lagrangian velocity spectrum and structure function under different PBL stability regimes generated by LES. *Physica A*, **389**, 4009–4017, https://doi.org/10.1016/j.physa.2010.05.059.

Salesky, S. T., M. Chamecki, and E. Bou-Zeid, 2017: On the nature of the transition between roll and cellular organization in the convective boundary layer. *Bound.-Layer Meteor.*, **163**, 41–68, https://doi.org/10.1007/s10546-016-0220-3.

Schmidt, H., and U. Schumann, 1989: Coherent structure of the convective boundary layer derived from large-eddy simulations. *J. Fluid Mech.*, **200**, 511–562, https://doi.org/10.1017/S0022112089000753.

Sullivan, P. P., and E. G. Patton, 2011: The effect of mesh resolution on convective boundary layer statistics and structures generated by large-eddy simulation. *J. Atmos. Sci.*, **68**, 2395–2415, https://doi.org/10.1175/JAS-D-10-05010.1.

Tatarskii, V. I., 1961: *Wave Propagation in a Turbulent Medium*. Dover, 285 pp.

van der Linden, S. J. A., and Coauthors, 2019: Large-eddy simulations of the steady wintertime Antarctic boundary layer. *Bound.-Layer Meteor.*, **173**, 165–192, https://doi.org/10.1007/s10546-019-00461-4.

van Heerwaarden, C. C., J. P. Mellado, and A. De Lozar, 2014: Scaling laws for the heterogeneously heated free convective boundary layer. *J. Atmos. Sci.*, **71**, 3975–4000, https://doi.org/10.1175/JAS-D-13-0383.1.

——, B. J. H. van Stratum, T. Heus, J. A. Gibbs, E. Fedorovich, and J. P. Mellado, 2017: MicroHH 1.0: A computational fluid dynamics code for direct numerical simulation and large-eddy simulation of atmospheric boundary layer flows.

Geosci. Model Dev., **10**, 3145–3165, https://doi.org/10.5194/gmd-10-3145-2017.

Wainwright, C. E., T. A. Bonin, P. B. Chilson, J. A. Gibbs, E. Fedorovich, and R. D. Palmer, 2015: Methods for evaluating the temperature structure-function parameter using unmanned aerial systems and large-eddy simulation. *Bound.-Layer Meteor.*, **155**, 189–208, https://doi.org/10.1007/s10546-014-0001-9.

Wilson, C. J., and E. Fedorovich, 2012: Direct evaluation of refractive-index structure functions from large-eddy simulation output for atmospheric convective boundary layers. *Acta Geophys.*, **60**, 1474–1492, https://doi.org/10.2478/s11600-012-0063-3.

Wyngaard, J. C., 2010: *Turbulence in the Atmosphere*. Cambridge University Press, 393 pp.

——, and M. A. LeMone, 1980: Behavior of the refractive index structure parameter in the entraining convective boundary layer. *J. Atmos. Sci.*, **37**, 1573–1585, https://doi.org/10.1175/1520-0469(1980)037<1573:BOTRIS>2.0.CO;2.

——, Y. Izumi, and S. A. Collins Jr., 1971: Behavior of the refractive-index-structure parameter near the ground. *J. Opt. Soc. Amer.*, **61**, 1646–1650, https://doi.org/10.1364/JOSA.61.001646.